7-21-2022

Automatic Data Aggregation to Assist in the Systematic Classification of Small Lunar Craters

Liam Powers
Ursinus College, lipowers@ursinus.edu

Automatic Data Aggregation to Assist in the Systematic Classification of Small Lunar Craters L. Powers[1]
[1]Ursinus College (Pfahler Hall, 601 E. Main Street, Collegeville, PA 19426, lipowers@ursinus.edu).

Introduction: Crater counting and classification are foundational to many techniques by which the surfaces of planetary bodies are characterized. Without physical samples from these bodies, analysis of their morphologies is one of the best methods available for understanding these surfaces. However, research has shown that differences in crater counting methods between different crater counting procedures—and even for repeated counts by the same counter—yield variable results.[1] This is likely unavoidable, but are there steps that we can take to make our crater counts as repeatable and transparent as possible, given these inherent limitations?

In this work, we consider the properties that human counters use to determine whether features are craters, as well as what properties have been used in the literature to classify small primary vs. secondary craters on the Moon. We then attempt to capture some of the key elements of this human decision-making by aggregating data that can be automatically extracted from a variety of lunar datasets based on an ellipse that is fit to a crater rim during the counting process. We also develop a process of automatically generating elevation profiles of craters >.5km in diameter.

While it is unlikely that this automatic data aggregation will be able to replace the counting and classification of human counters, we hope to develop a tool that will allow us to provide more systematic, quantitative rationale for our human classifications, allowing us to be more transparent and repeatable in our crater classifications and counts.

Methods: In developing our data aggregation system, we have considered the ways in which human counters identify craters and what properties have been used by previous workers to distinguish small primary craters from secondary craters. For example, a human counter who is searching for small, fresh lunar primary craters is likely to look for features with circular planforms, raised rims, and depth to diameter ratios of ~1/5.[2] The presence of a well-preserved, azimuthally symmetric continuous ejecta blanket would indicate a recent impact from near normal, while an up-range zone of avoidance in the ejecta blanket or a "butterfly" ejecta pattern would suggest progressively more oblique impact conditions.[3]

A variety of datasets have been used in the literature to characterize the shape of continuous ejecta and crater rays. Rays and continuous ejecta are evident as albedo features in visible wavelength imagery.[4] Optical maturity also reveals the presence of rays and continuous ejecta, given that for fresh craters, they are composed of optically immature material.[4] Similarly, the rocky ejecta blankets of fresh craters may present as elevated rock abundance features in thermal measurements.[5]

Secondary craters that form at relatively low velocities near their parent craters are often also identified by human crater counters on the basis of their morphology. "Classic" secondary crater morphologies include elliptical planforms, shallow depths relative to crater diameters, v-shaped uprange dunes, downrange braided or textured surfaces, and dense spatial clustering.[6] While secondary craters that form further from their parent craters may produce deeper craters relative to their diameters and more circular planforms due to higher impact speeds, workers have identified even these secondary craters on the basis of properties such as spatial clustering.[1] Downrange "tails" of anomalous thermal inertia and radar CPR have also been recorded in association with distal secondary craters.[7]

Our goal is to automatically extract and aggregate quantitative data that is representative of these kinds of observations, as they are often implicitly gathered by human counters during the process of classification.

Data: A test population comprised of 48 pre-selected, well-defined primary and secondary craters ranging between 0.6-4 km that were located near Tycho secondary crater chains with classic secondary crater morphologies. Tycho was selected for study because its well-preserved secondary population has been characterized by other workers, employing a variety of datasets.[6,8-14]

We defined the size of our craters by fitting an ellipse to their rims using the "5-pt Ellipse" tool in the JMARS desktop software program.[15] The major axis of this ellipse was used as our crater diameter. Data for each crater was extracted from the "Clementine UVVIS/Optical Maturity - Numeric" (128 PPD)[16,], "Rock Abundance (Full Mission)" (128 PPD)[5,11], and "Blended LRO/LOLA and SELENE/Kaguya DEM"[17] layers that are available in the JMARS, as well as from a layer of Arecibo-GBT ground based 12.6 cm radar CPR data that was obtained from the Planetary Data System and imported into JMARS.[18]

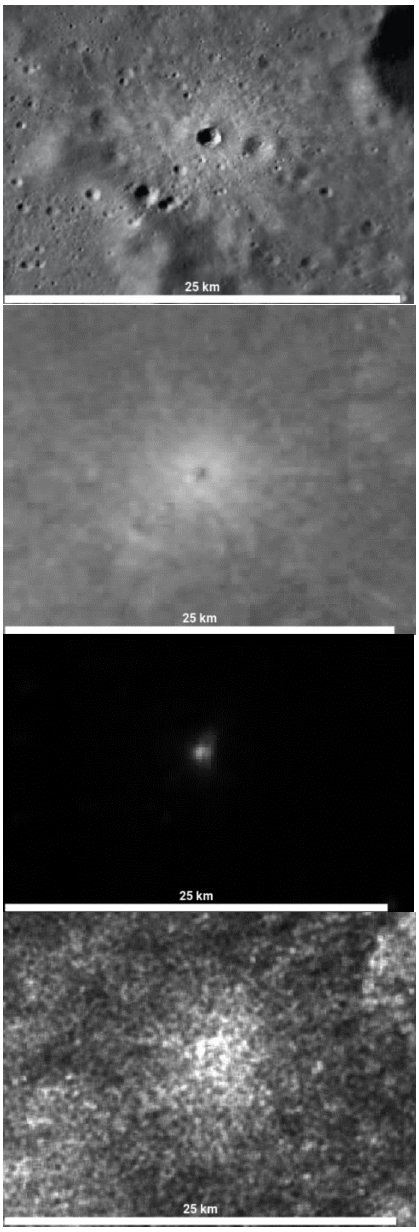

Figure 1: Example datasets' coverage of a primary crater from test population on the Moon, located at -33.717°N, 17.242°E, taken from within the JMARS software. Datasets in order from top to bottom are: LROC WAC Global 100m/px, Clementine UVVIS/Optical Maturity – Numeric, Rock Abundance (Full Mission), and Arecibo-GBT ground based 12.6 cm radar CPR.

These data were extracted from JMARS using the Map Sampling tool, outputting the average pixel value of the region within the area of the ellipse that was created during counting. This method was also used over two additional circles created over the initial ellipse, with sizes of 1.5 and 2.5 crater radii with respect to the original crater, in order to analyze the possible ejecta blanket of these craters. These data were in turn paired into multiple sets and analyzed. Average pixel values were calculated from the region between the smaller circle and the ellipse, and between the smaller circle and the larger circle. This provided a relative pixel value of the background terrain around the crater. Ratios were then constructed comparing the ellipse values to both the inner and outer circle averages. These automated calculations were performed for each crater in the test population, and for each of the optical maturity, rock abundance, and radar polarization datasets. Future work might include additional datasets that show promise in identifying differences between primary and secondary craters.

Elevation profiles were extracted from the Blended LRO/LOLA and SELENE/Kaguya DEM layer along four transects of each crater at 45 degree azimuthal spacing. Each profile consists of a line of points spaced 105m apart that extends beyond the crater diameter extracted from the initial ellipse, with each point extracting the elevation value from the DEM elevation layer. Plots were then constructed from these elevation profiles, with a non-linear 6-term gaussian least-squares fit curve plotted to each of the four raw profiles. The 4 raw-data profile plots and the 4 gaussian plots were then averaged separately, with a separate plot created for these averages, as shown in Figure 2. Depth-to-diameter ratios were then calculated from these gaussian plots for each crater.

In future work, the relative degree of clustering of each crater will also be computed. Together, these measurements will help to capture some of the key components that human counters use to distinguish between the morphology of secondary craters and small primary craters.

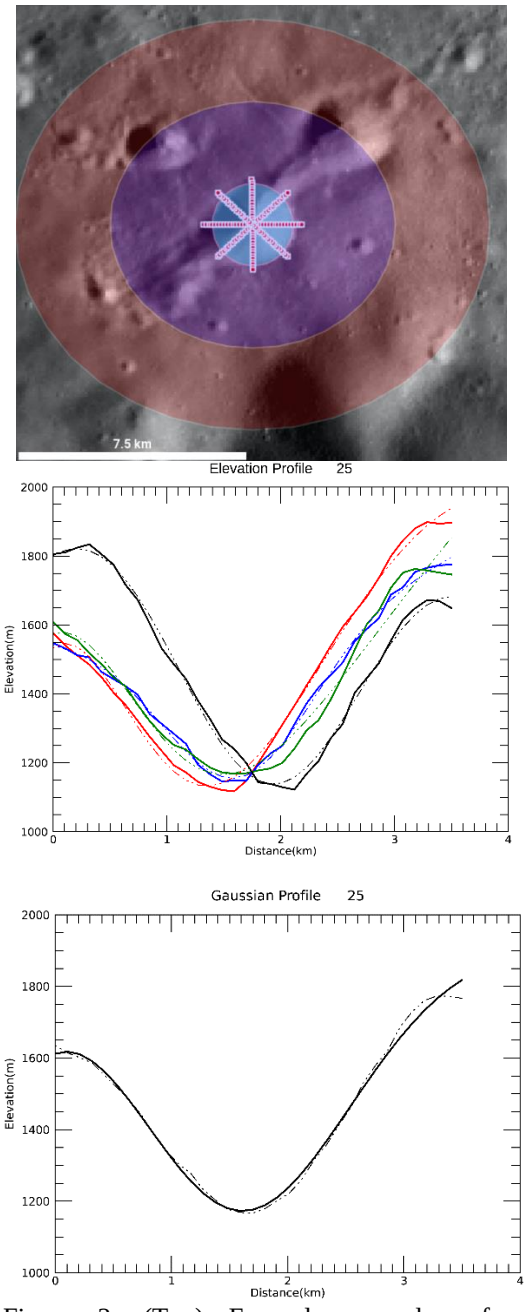

Figure 2: (Top) Example secondary from test population, located at -30.3308°N, 18.1417°E, with ellipse overlay in teal, small circle in blue, large circle in red, and elevation profiles shown in red points. (Middle) Elevation profile plot of the data extracted from said points, with each transect plotted in a different color; red, blue, green, or black. Gaussian fits are calculated and plotted for each individual transect and plotted, shown in the dotted curve of the same color. (Bottom) The average of the 4 gaussian profile plots is plotted in the solid black curve, and the average of the raw-data profiles is plotted in the dotted curve to show agreement between the two.

Analysis: From our test population, ideal primary and secondary candidates were selected for analysis. For example, the crater shown in Figures 1 and 3, which was counted as a primary, returned a depth-to-diameter ratio of ~1/5, which is expected for primaries of that size. For inner-to-outer circle ratios (blue region values/red region values as shown in Figure 2), calculations returned 1.20032, 1.30148, and 5.15021 for CPR, optical maturity, and rock abundance data respectively. For ellipse-to-outer ratios (teal values/blue+red values), calculations returned 0.910479, 0.969979, and 0.787705 for CPR, optical maturity, and rock abundance data respectively. The closer a given value is to 1, the more similar the data in the compared regions is. Values of ~1 show a high level of agreement between compared regions, while values greater than or less than 1 indicate differences in pixel averages, the further away from 1, the more significant the difference. For an ideal primary ejecta blanket, as shown here, a definable difference between material in the crater basin, ejecta blanket and surrounding local terrain is expected based on our assumptions. This is encouraging, as our data show distinct, measurable differences in the case of this primary.

Data was also analyzed for the crater in Figure 2, which was counted as a secondary. For inner-to-outer ratios, calculations returned ratios of 1.10721, 1.09948, and 1.13895 for CPR, optical maturity, and rock abundance data respectively, and ellipse-to-outer ratios returned 0.92047, 0.89766, and 0.829319 for CPR, optical maturity, and rock abundance data respectively. Again, our model was able to detect a definable difference between the crater, the immediate ejecta blanket, and the surrounding terrain.

However, this is an ideal test case. As seen in Figure 2, the generated circles that encompass the ellipse count often include other small craters from the region, especially in the case of clustered secondaries, like Figure 2 depicts. Should a small primary be included in one of those outer regions, is could heavily skew the average calculations of the region. Calculations are also limited by the resolution of extracted datasets, with most being limited to 1024PPD, which roughly equates to one pixel per 200m^2 on the Moon, and in dealing with sufficiently small craters or craters with little definable difference between the crater basin and their surrounding terrain, this low-resolution data presents an obstacle.

This emphasizes the preliminary aspect of this work, and reiterates the need for human review of recommendations that might be generated by these calculations at this time.

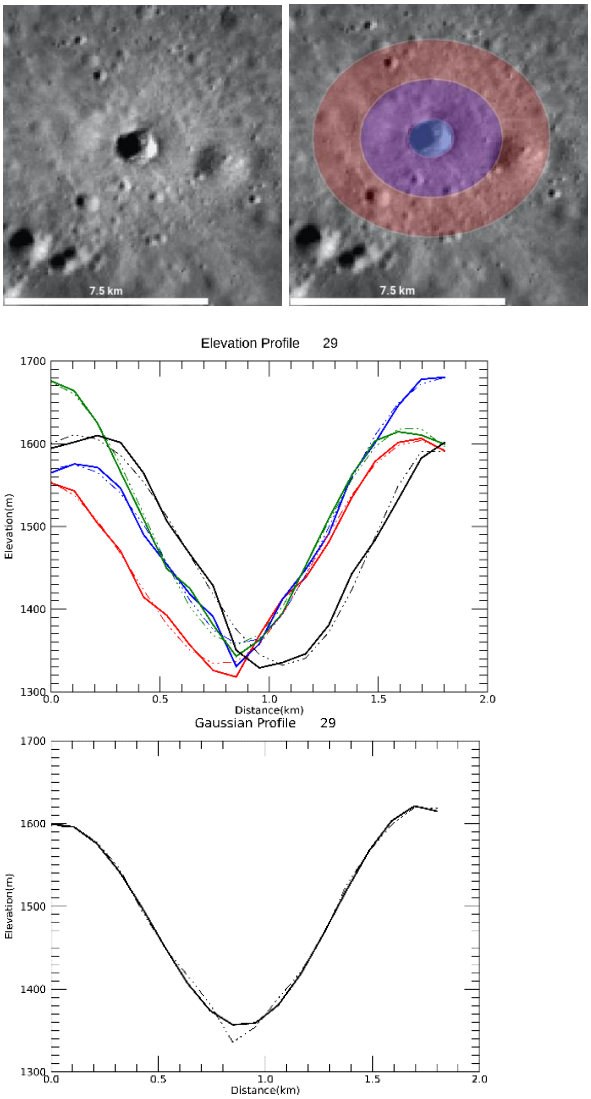

Figure 3: (Top) Example primary from Figure 1 with visible ejecta blanket and shape overlays show coverage of the ejecta blanket. (Middle) Elevation plot of example primary from Fig.1. (Bottom) Averages plot of example primary from Fig.1.

Conclusions: While this preliminary work is limited in its scope, these initial data show promise in their ability to identify craters, and aggregate data significant to their classification. Definable differences in extracted data for both primaries and secondaries show potential usefulness in the development of a recommendation system for human counters. The method of automatically extracting elevation profiles on a per-crater basis provides a promising addition to this data, though further work is required to refine the automatic creation of depth-to-diameter ratios.

Other difficulties that remain to be addressed include the differences in registration of the different datasets in JMARS, which skews the results of automatic data extraction based on the ellipse centers fit relative to the LROC WAC and NAC data. However, with further testing and development, we hope to produce a systematic data aggregation and recommendation procedure that will make our crater counts and classifications more transparent and repeatable.

Acknowledgments: I gratefully acknowledge the JMARS software and associated PDS data products, and the support of my advisor, Dr. Kassandra Martin-Wells, without which this work would not have been possible.

References: [1] Robbins, S.J., et al. (2014) *Icarus, 234*,109-131. [2] Melosh, H.J. (1989) *Oxford University Press.* [3] Herrick, R.R. and Forsberg-Taylor, N.K. (2003) *Meteorics & Planet. Sci., 38*, 1551-1578. [4] Hawke, B.R. et al. (2004) *Lunar and Planet. Sci. Conference LX*. [5] Bandfield, J.L., et al., (2011), *J. Geophys. Res. 116*, E12. [6] Lucchitta, B.K.(1976) *Icarus, 30*, 80-96. [7] Martin-Wells, K.S. et al. (2017) *Icarus, 291*, 176-191. [8] Campbell, B.S., et al. (1992) *Proc. Lunar Planet. Sci. Conf. 22nd*, 259-274. [9] Plescia, J.B. and Robinson (2019) *Icarus, 321*, 974-993. [10] Krüger, T., van der Bogert, C.H. and Hiesinger, H. (2016) *Icarus, 273*, 164-181. [11] Bandfield, J.L. et al. (2017) *Icarus, 283*, 282-299. [12] Dhingra, D., Head, J.W. and Pieters, C.M. (2017) *Icarus, 283*, 268-281. [13] Zanetti, M. et al. (2017) *Icarus, 298*, 64-77. [14] Bray, V.J. et al. (2018) *Icarus, 301*, 26-36. [15] H. Riris, J. et al. (2017) *Proc. SPIE 10565, International Conference on Space Optics — ICSO* 2010. [16] Lucey, P. G., G. J. Taylor, and E. Malaret, (1995), *Science, 268*, 1150-1153. [17] Barker, M.K., et al. (2016) *Icarus, 273* 346-355. [18]Campell, B. A., (2010) *Icarus, 208*, 565-573.